Journal of Catalysis **212,** 56–62 (2002)
doi:10.1006/jcat.2002.3778

Effect of Gold on the HDS Activity of Supported Palladium Catalysts

A. M. Venezia,*,[1] V. La Parola,† V. Nicolì,† and G. Deganello*,†

*Istituto per lo Studio dei Materiali Nanostrutturati, ISMN-CNR Sezione di Palermo, via Ugo La Malfa 153, 90146, Palermo, Italy; and †Dipartimento di Chimica Inorganica e Chimica Analitica "S. Cannizzaro", Università di Palermo, Viale delle Scienze, Parco D'Orleans, 90128, Palermo, Italy

Received July 5, 2002; revised July 29, 2002; accepted July 31, 2002

The effect of gold on palladium catalysts supported on amorphous aluminosilicate was investigated in the hydrodesulfurization of thiophene. A series of bimetallic Au_xPd_y catalysts was prepared by the slow deposition–precipitation method with decomposition of urea. The structural and surface properties of the samples were analyzed by X-ray diffraction and X-ray photoelectron spectroscopy techniques at different stages of the catalyst life. After calcination at 673 K, gold-enriched solid solutions of approximately $Au_{90}Pd_{10}$ and $Au_{80}Pd_{20}$ composition were formed for all samples of different Au/Pd ratios, along with free palladium phases. $Au_{80}Pd_{20}$ was the prevailing phase. Hydrogen treatment of the catalyst at 673 K before catalytic tests reduced free palladium oxide to free metallic Pd. An increase of the hydrodesulfurization activity with increasing gold amount up to 50 wt% was found. The structural analysis of the "aged" catalysts indicated formation of palladium sulfide, Pd_4S, in the monometallic palladium and in the bimetallic palladium-rich samples but not in the gold-rich samples. The catalytic behavior of the catalysts was related to the formation of the Au_xPd_y clusters and to the inhibition of the sulfide-phase formation.

Key Words: **Au–Pd catalysts; Au–Pd alloy phases; hydrodesulfurization; HDS; thiophene.**

1. INTRODUCTION

The increasing concern about environmental pollution promotes the current research in the field of petroleum hydrotreating processes toward the development of new catalysts for hydrodesulfurization (HDS), which consists of the removal of sulfur from petroleum feedstock (1). The actual HDS catalysts consisting of alumina-supported Mo and Co oxides have a tendency to deactivate by coke formation and are not able to lower the sulfur content down to the limit of 50 ppm imposed by new legislation (2, 3). In particular, the inefficiency of these catalysts is more severe in the presence of polyaromatic compounds, which are hard to desulfurize because of the extra stabilization given by the aromatic rings. In addition to the sulfur problem, health hazards associated with aromatics (4), specially in the case of diesel fuels, are causing new limitations to be being introduced. Different approaches based on noble metals are currently being tried in an attempt to achieve efficient hydrodesulfurization and hydrogenation of aromatics (5, 6). These catalysts are suitable for deep aromatics saturation but are easily poisoned by small amounts of sulfur in the feedstock (7, 8). The sulfur tolerance of these catalysts may be increased by the addition of a transition metal promoter and also by the acidity of the support (9, 10).

Two pathways have been suggested for the mechanism for the HDS of thiophenes, both leading to butene formation. One route involves a C–S cleavage with direct extrusion of sulfur and the formation of intermediate butadienes; the other path involves a prehydrogenation followed by C–S bond rupture with formation of intermediate tetrahydrothiophene. The relative contribution of each pathway is determined by the reaction conditions, by the type of substrate, and by the catalyst (2). Palladium is a well-known hydrogenation catalyst, but only recently has it been shown that Pd(111) can directly activate the thiophene decomposition, resulting in the deposition of sulfur and the formation of C_4 species on the surface (11). Gold catalysts have also received growing interest due to the surprisingly high catalytic activity exhibited in many reactions of industrial and environmental importance, such as the low-temperature oxidation of CO and the epoxidation of propylene (12–15). Quite relevant to the present research on HDS catalysts is the strong affinity of gold with sulfur compounds, currently exploited in gas sensors for the detection of H_2S and also in molecular electronics using the specific bonding between Au- and sulfur-containing functional groups (13, 16). An important requisite to achieving good catalytic activity is the nanoscale structure of the supported gold particles by means of various preparation techniques. Moreover, the addition of gold to palladium catalysts has been recently found to improve the activity and selectivity in hydrogenation reactions (17) and in hydrodechlorination (18, 19). Based on the above considerations, we selected both metals, Pd and Au, as good candidates for catalysts in hydrotreatment processes. A major drawback for using palladium, consisting of sulfur poisoning, could be removed or minimized by the use of a second metal, like gold, capable of forming solid

[1] To whom correspondence should be addressed. Fax: ++390916809399. E-mail: anna@ictpn.pa.cnr.it.

0021-9517/02 $35.00

solutions. Recent studies on Pt catalysts have indeed shown that addition of a second noble metal, such as Pd, improves the resistance to sulfur (20).

With the aim of developing new suitable systems for HDS reactions, a series of Pd catalysts supported on amorphous aluminosilicate (ASA) containing different amounts of gold and with a total metal content of 2 wt% was prepared by slow deposition–precipitation methods and was characterized by X-ray diffraction and XPS spectroscopy. The effect of gold on the catalytic activity in the HDS of thiophene was evaluated and related to the structural changes of the catalysts and to the presence of bimetallic clusters, Au_xPd_y, of different composition.

2. EXPERIMENTAL

2.1. Catalyst Preparation

Monometallic Pd/ASA and Au/ASA and bimetallic Au–Pd/ASA catalysts with a total metal loading of 2 wt% were prepared by a deposition–precipitation method (21). In accordance with this procedure, urea in a molar ratio of 4 : 1 with respect to the metals was added to an aqueous suspension of the support (ASA constituted of 86% SiO_2, 13% Al_2O_3, and minor oxide components; surface area of 430 m^2/g; pore volume of 0.92 ml/g) containing the dissolved precursor salts $PdCl_2$ or $HAuCl_4 \cdot 3H_2O$ in the appropriate amounts. By heating to 363 K, urea decomposed, generating OH^- ions, which precipitated the metal hydroxides on the surface of the support acting as a nucleating agent. The solution (pH of 6) was kept refluxing and under stirring for 18 h. The excess water was removed in a rotary evaporator and the solid was washed several times in order to eliminate the chloride ions. Finally the samples were dried in an oven at 343 K and then calcined in air at 673 K. All reagents were from Aldrich Chemical Co. The prepared catalysts are listed in Table 1. The numbers in the sample notation refer to the relative weight percentages of the metals.

TABLE 1

Rate Constants (k), Activation Energies (E_{act}), and Deactivation Percentages (% d), of the ASA-Supported Catalysts in the HDS of Thiophene

Catalysts	k (ml/$g_{cat} \cdot s$)	E_{act} (kJ mol^{-1})	% d
Pd	0.18	52	65
$Au_{10}Pd_{90}$	0.19	37	71
$Au_{25}Pd_{75}$	0.21	30	71
$Au_{35}Pd_{65}$	0.19	53	65
$Au_{50}Pd_{50}$	0.19	37	75
$Au_{65}Pd_{35}$	0.13	42	64
$Au_{75}Pd_{25}$	0.11	62	56
$Au_{90}Pd_{10}$	0.037	61	84
Au	0.011	43	83

2.2. Catalyst Characterization

2.2.1. XRD. The X-ray diffraction measurements for the structure determination were carried out with a Philips vertical goniometer using Ni-filtered Cu $K\alpha$ radiation. A proportional counter and a 0.05° step size in 2θ, from $2\theta = 30°$ to 50°, were used. The assignment of the various crystalline phases was based on the JPDS powder diffraction file cards (22). The obtained XRD profiles were fitted using the software provided with the instrument. From the lattice parameter shifts, calculated from the angular position of the (111) and (200) metal reflections, according to Vegard's law, the compositions x and y of the solid solutions Au_xPd_y were obtained (23). The particle sizes of different phases were calculated from the line broadening of the most intense reflections using the Scherrer equation (24).

2.2.2. XPS. The X-ray photoelectron spectroscopy analyses were performed with a VG Microtech ESCA 3000 Multilab, equipped with a dual Mg/Al anode. The spectra were excited by the nonmonochromatized Al $K\alpha$ source (1486.6 eV) operated at 14 kV and 15 mA. The analyzer operated in the constant analyzer energy (CAE) mode. For the individual peak energy regions a pass energy of 20 eV across the hemispheres was used. Survey spectra were measured at a 50-eV pass energy. The sample powders were pelletized and then mounted on double-sided adhesive tape. The pressure in the analysis chamber was in the range of 10^{-8} Torr during data collection. The constant charging of the samples was corrected by referencing all the energies to the C 1s peak at 285.1 eV arising from adventitious carbon. The invariance of the peak shapes and widths at the beginning and at the end of the analyses indicated the absence of differential charging. The peaks were fitted by a nonlinear least-squares fitting program using a properly weighted sum of Lorentzian and Gaussian component curves after background subtraction, according to Shirley (25) and Sherwood (26). For the exact determination of the Pd $3d_{5/2}$ and Au $4f_{5/2}$ binding energies, the overlapping Au $4d_{5/2}$ and Pd 4s peaks were included in the fitting procedure. The binding energy (BE) values are quoted with a precision of ±0.15 eV. Contact of the samples with air was minimized during sample loading; in particular for the catalysts after the HDS reaction, the sample preparation procedures were carried out inside a nitrogen-filled glove bag.

2.3. Catalytic Activities

The hydrodesulfurization of thiophene was carried out in the vapor phase using a continuous flow microreactor (27). An amount of 200 mg of the catalyst (sieved fraction, 210–430 μm), diluted with inert particles of SiC, in order to limit the radial thermal gradient, was placed inside a quartz reactor (8 mm ∅). Prior to the HDS measurements the catalyst was treated for 1 h in flowing H_2 (25.7 ml/min) while the temperature was raised to 673 K at a heating rate of 7 K/min.

Thereafter the reactor was cooled to the reaction temperature of 613 K under flowing (30 ml/min) N_2. Meanwhile, by letting H_2 flow through a vessel containing thiophene at 283 K, a gas mixture of 5.2 vol% thiophene in H_2 was obtained. This mixture was directed into the reactor at atmospheric pressure at a flow rate of 25.7 ml/min. The products were analyzed by gas chromatography with a Carlo Erba GC 8340 chromatograph equipped with a packed column, 2 m × 5 mm, filled with squalene, at the oven temperature of 343 K using a flame ionization detector. The data were collected at 25-min intervals over a period of 16 h. The chromatogram contained peaks corresponding to the C_4 products and to unreacted thiophene. The different components of C_4 were not separated; therefore only the total C_4 signal was considered in the activity calculations. The fractional conversion was calculated from the ratio of the peak area of the products over the sum of the peak areas of products and thiophene. Typically the catalysts deactivated during the time on stream until a plateau of steady-state conditions was reached, after about 8 h. The rate constants (k_{HDS}) per gram of catalyst of the pseudo-first-order HDS reaction of thiophene for this series of catalysts, was determined using the integral reactor equation

$$k_{HDS} = -\ln(1-x)F_0/W,$$

where x is the fractional conversion at the steady-state conditions, F_0 (ml s^{-1}) the volumetric reagent gas flow, and W the weight of the catalysts (g). From the initial conversion x_i considered after 2 min of time on stream, and conversion at stationary conditions x_f, a percentage of initial deactivation % d was calculated as

$$\% d = 100 \cdot (x_i - x_f)/x_i$$

(27). Measurements of the rate constants at three different temperatures (613, 628, and 643 K) allowed determination of the activation energy for each catalyst. The absence of deactivation during the measurements at different temperatures was checked for by experiments of ascending and descending temperature. The error on the catalytic activity data, such as rate constants and activation energies, was estimated as 10%, mostly arising from the oven temperature fluctuation.

3. RESULTS

The catalytic results for the thiophene HDS reaction, in terms of rate constant, activation energy, and deactivation percentage, for our catalysts are reported in Table 1. As expected from the study by Pecoraro and Chianelli on the HDS activity of several transition metal sulfides, a monometallic palladium catalyst exhibits fair activity (28). A slight increase in the rate constant is observed from pure palladium catalyst to the bimetallic $Au_{50}Pd_{50}$, followed by a decline for the samples with higher gold loadings. The activation energies and the initial deactivation percentages do not exhibit a particular trend with metal composition. Whereas the variation of the deactivation values are within experimental error, changes in the activation energies are definitely larger than the experimental error. Overall, the activation energies are smaller than the recently reported values for ASA-supported CoMo catalysts (27). Considering palladium to be the active metal in the system under study, the experimental rate constants were normalized with respect to the palladium content. The obtained values were then reported versus gold content, as shown in Fig. 1. With an increasing amount of gold up to 50 wt%, a steady increase in the rate constant expressed per unit mass of Pd is observed. Thereafter, a plateau is reached for the high-gold-loaded samples.

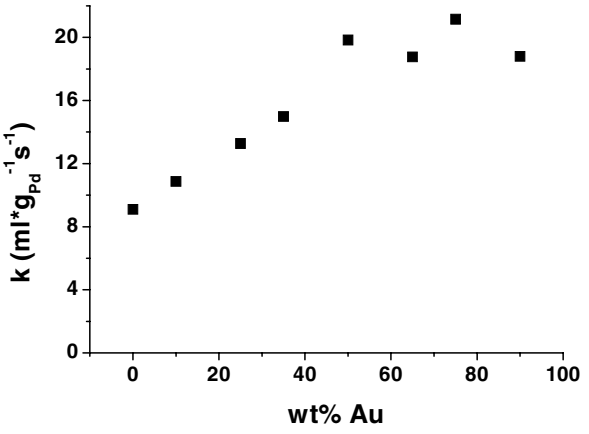

FIG. 1. Variation in the rate constant, obtained at 613 K, normalized to palladium weight, versus the weight percent of Au for the ASA-supported Au_xPd_y catalysts.

X-ray diffraction patterns of the monometallic and bimetallic catalysts in the range of 30°–42° 2θ are shown in Fig. 2. For the monometallic palladium sample, the (101)

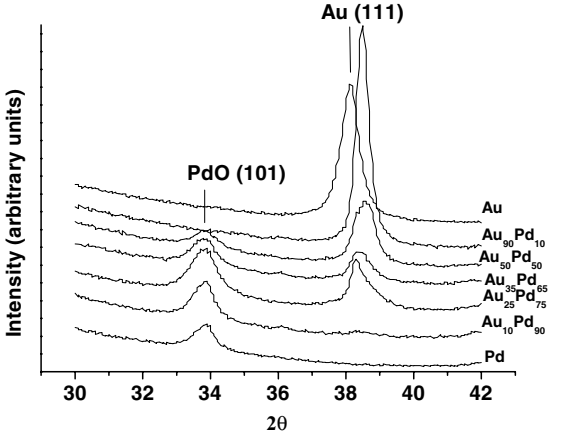

FIG. 2. X-ray diffractograms of the monometallic and bimetallic catalysts after calcination at 673 K.

TABLE 2

Crystal Phases of the Mono- and Bimetallic Samples after Calcination at 673 K

Catalysts	Crystal phases (size in Å)
Au	Au (250)
$Au_{90}Pd_{10}$ ($Au_{84}Pd_{16}$)	$Au_{81}Pd_{19}$ (240)
$Au_{75}Pd_{25}$ ($Au_{62}Pd_{38}$)	$Au_{78}Pd_{22}$ (200), 95%; PdO (100), 5%
$Au_{65}Pd_{35}$ ($Pd_{50}Au_{50}$)	PdO (100), 13%; $Au_{92}Pd_{8}$ (900), 4%; $Au_{79}Pd_{21}$ (180), 83%
$Au_{50}Pd_{50}$ ($Au_{35}Pd_{65}$)	PdO (110), 25%; $Au_{90}Pd_{10}$ (400), 10%; $Au_{78}Pd_{22}$ (100), 65%
$Au_{35}Pd_{65}$ ($Au_{23}Pd_{77}$)	PdO (114), 51%; $Au_{91}Pd_{9}$ (340), 9%; $Au_{76}Pd_{24}$ (130), 40%
$Au_{25}Pd_{75}$ ($Au_{15}Pd_{85}$)	PdO (100), 55%; $Au_{91}Pd_{9}$ (350), 11%; $Au_{79}Pd_{21}$ (150), 34%
$Au_{10}Pd_{90}$ ($Au_{06}Pd_{94}$)	PdO (130)
Pd	PdO (120), 93%; Pd (360), 7%

Note. The corresponding crystal particle sizes are reported in parentheses, with the relative molar percentages. In the first column the composition of the samples on a molar basis are reported.

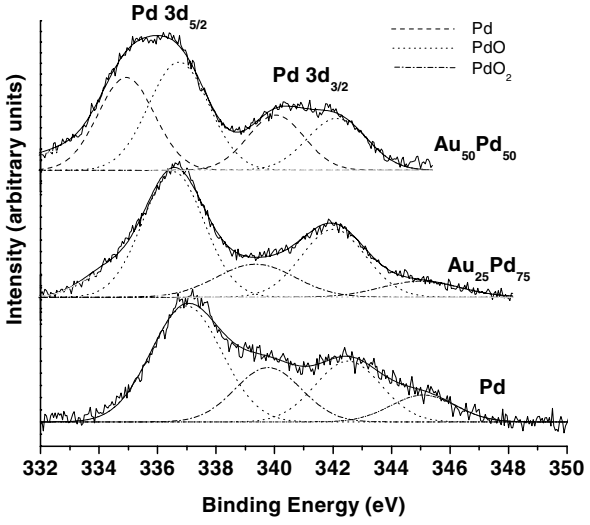

FIG. 3. Experimental and fitted Pd 3d photoelectron spectra of monometallic palladium and bimetallic catalysts after calcination at 673 K.

reflection of the PdO oxide phase is present. The gold catalyst exhibits the most intense (111) reflection, typical of pure metallic gold. This line is shifted toward higher 2θ in most of the bimetallic diffractograms, with the exception of the $Au_{10}Pd_{90}$ diffractogram, where this reflection is absent. With increasing gold content, the PdO lines decrease in intensity up to complete disappearance in the $Au_{90}Pd_{10}$ sample. More-detailed analyses of the diffraction patterns, involving fitting of the experimental data and evaluation of the lattice parameters, allowed discrimination between different Au_xPd_y solid solutions with the corresponding particle sizes and the relative metal percentages. The structural data are reported in Table 2. The compositions of the bimetallic samples on a molar basis are also reported, in parentheses in the catalyst column. By looking at the data, it appears that gold has the tendency to capture palladium in its lattice, forming solid solutions rich in gold. The occurrence of two solid solutions of approximate compositions $Au_{80}Pd_{20}$ and $Au_{90}Pd_{10}$ is worth noticing.

The surface properties and possible preferential segregation of one of the two metals were investigated by X-ray photoelectron spectroscopy. The experimental and fitted Pd 3d spectra of selected samples after calcination are shown in Fig. 3. The Pd 3d spectra, characterized by the two spin–orbit components, Pd $3d_{5/2}$ and Pd $3d_{3/2}$, separated by 5.4 eV, exhibit two doublets attributed to different chemical species. The concentration of each species is affected by the amount of gold. According to the literature, the highest Pd $3d_{5/2}$ energy value (339.5 eV) is attributed to PdO_2, likely formed during air calcination (29). The component at around 337 eV is due to PdO, whereas the component at 335.0 eV is due to metallic palladium (29). With an increasing amount of gold, PdO_2 disappears completely and the metallic palladium peaks increase with respect to those of the PdO species. The binding energy values of the Pd $3d_{5/2}$, Au $4f_{7/2}$, Si 2p, and O 1s peaks are listed in Table 3. Si 2p and O 1s binding energies are typical of silicon and oxygen of the support (30). Gold binding energies are typical for the metallic state (29, 31). A negative shift (about 0.5 eV) of the Au $4f_{7/2}$ binding energy for the bimetallic catalysts with respect to the monometallic Au catalyst is observed, in agreement with literature data (32). The shift could be attributed to a charge transfer from Pd to Au on the grounds of the bulk electronegativity differences and could be indicative of alloy formation (33). In contrast, the observed Pd 3d binding energy shifts are mainly due to oxidation

TABLE 3

Principal Binding Energy Values of the XPS Peaks of the Various Catalysts

Catalysts	Pd $3d_{5/2}$	Au $4f_{7/2}$	Si 2p	O 1s
Pd	337.1 (3.0), 70% 339.8 (2.1), 30%		103.5 (2.5)	532.5 (2.6)
$Au_{10}Pd_{90}$	336.8 (3.5)	84.0 (2.0)	103.6 (2.4)	532.6 (2.6)
$Au_{25}Pd_{75}$	336.7 (2.4), 76% 339.6 (3.2), 24%	83.8 (2.0)	103.5 (2.4)	532.4 (2.7)
$Au_{35}Pd_{65}$	335.9 (3.2), 27% 337.1 (2.2), 73%	84.0 (2.0)	103.8 (2.4)	532.8 (2.7)
$Au_{50}Pd_{50}$	335.0 (2.3), 60% 336.8 (2.4), 40%	84.1 (1.6)	103.5 (2.3)	532.4 (2.6)
$Au_{75}Pd_{25}$	335.3 (3.0)	83.9 (2.0)	103.6 (2.4)	532.7 (2.7)
Au		84.4 (1.6)	103.5 (2.7)	532.5 (2.8)

Note. The full widths at half maximum are given in parentheses. In the presence of multiple palladium species, the relative percentages of the components are also reported.

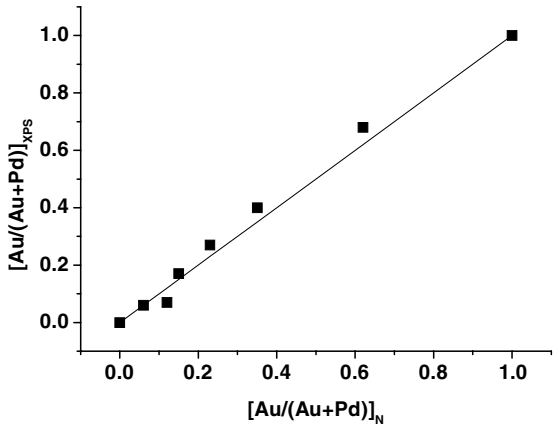

FIG. 4. XPS-derived atomic ratios versus nominal ratios of the Au_xPd_y catalysts. Solid line corresponds to the perfect agreement between the two sets of values.

state change. The atomic ratios $[Au/(Au + Pd)]_{XPS}$, as derived from XPS versus the corresponding nominal ratios $[Au/(Au + Pd)]_N$, are shown in Fig. 4. The comparison between the two sets of data indicates a slight surface segregation of gold, in agreement with its higher sublimation and surface energy compared to that of palladium (34).

The structural changes of the catalysts on the HDS reactions were also investigated by X-ray diffraction. The X-ray diffractograms of the monometallic Pd catalyst and the bimetallic catalysts of different Au/Pd compositions are reported in Fig. 5. The monometallic palladium sample is characterized by the presence of crystalline sulfide, Pd_4S. According to the phase diagram of the Pd–S system, Pd_4S is formed for very low H_2S/H_2 ratios (between 0.008 and 0.025), which is likely to occur under the current reaction conditions (35). The intensities of the related peaks decrease with the increase in gold content up to a complete disappearance in the bimetallic samples with more than 35% Au. The diffractograms of these samples present only the reflections due to the solid solutions.

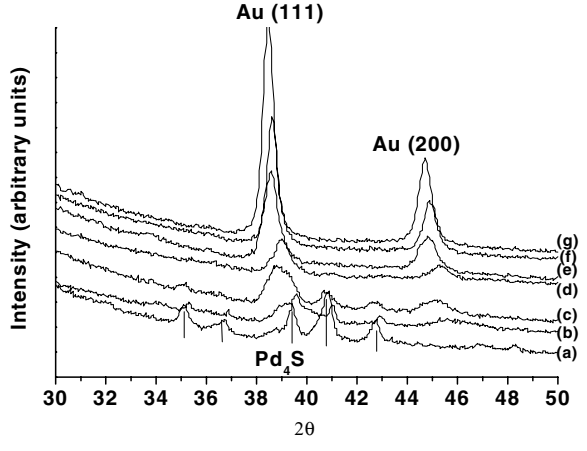

FIG. 5. X-ray diffractograms of various samples after HDS reaction: (a) Pd; (b) $Au_{25}Pd_{75}$; (c) $Au_{35}Pd_{65}$; (d) $Au_{50}Pd_{50}$; (e) $Au_{65}Pd_{35}$; (f) $Au_{75}Pd_{25}$; (g) $Au_{90}Pd_{10}$. The Pd_4S reflections are indicated by vertical lines.

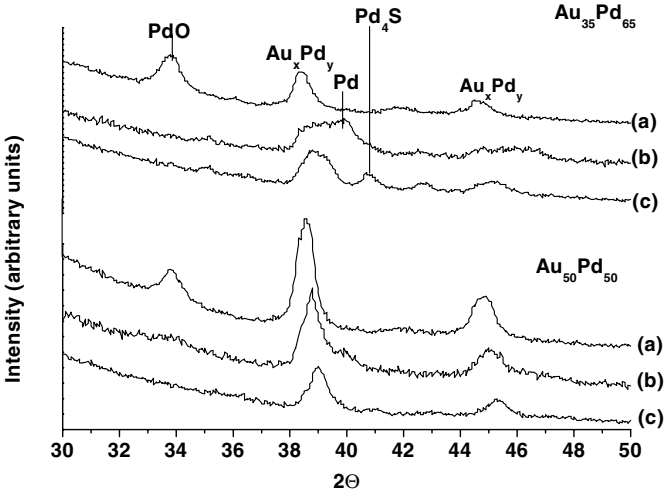

FIG. 6. X-ray diffractograms of the $Au_{35}Pd_{65}$ and $Au_{50}Pd_{50}$ samples after different treatments: (a) after calcination at 673 K; (b) after reduction in H_2 at 673 K; (c) after HDS reaction.

The structural variations, undergone in the different steps of their lives, by two catalysts with different metal percentages are summarized in Fig. 6. The changes seem to depend on the metal composition. On calcination, as observed in Fig. 2, PdO and Au_xPd_y solid solution are formed. After hydrogen treatment, the PdO is mainly reduced to metallic Pd. The subsequent HDS reaction determines the formation of Pd_4S. Comparison of the diffractograms of the two different samples suggests that the formation of the palladium sulfide arises mainly from the free metal palladium. Indeed for the $Au_{50}Pd_{50}$ sample, the X-ray pattern taken after hydrogen treatment exhibited a small reflection due to free Pd, whereas the diffractogram of the aged catalyst did not contain any peaks related to the sulfide phase. Analogously, for all the samples with Au $\geq$35% the corresponding diffractograms did not show any sulfide-related peaks.

4. DISCUSSION

The experimental results obtained from the hydrodesulfurization of thiophene evidenced a positive effect of gold on the catalytic activity of the ASA-supported palladium catalysts. The activity, expressed as rate constant per gram of palladium, increased steadily up to a gold loading of 50 wt%. Thereafter, a plateau was reached. The value of the rate constant at the plateau was larger with respect to the value of the monometallic palladium catalyst.

An explanation for the observed catalytic behavior can be found from the structural data of Table 2 referring to the calcined samples. The presence of gold determined

the formation of a true solid solution at the expense of free palladium oxide, even under oxidizing conditions. The obtained solutions were always gold enriched, regardless of the nominal composition of the samples. In particular, the analyses of the lattice parameters indicated the compositions of approximately $Au_{80}Pd_{20}$ and $Au_{90}Pd_{10}$ as the most likely structures. No direct relation between particle size and activity can be proposed from the current data. The palladium–gold system forms a solid solution in the whole range of composition; however, in the current case the adopted preparation procedure of the slow deposition–precipitation of metal hydroxides could have played an important role in determining the final alloy composition. In this method, the precursor to the active species is removed from the solution in the presence of a suspension of the support: the OH^- groups on the surface of the support may act as nucleating agents. On the basis of the solubility constants of $Au(OH)_3$ and $Pd(OH)_2$, which are equal to 3×10^{-6} and 3×10^{-30}, respectively (36), it is expected that under the pH conditions determined by the decomposition of urea, palladium hydroxide would precipitate away from the support surface, whereas gold hydroxide would slowly precipitate at the surface sites. The anchored gold, readily reduced to the metallic state, may have determined the composition of the solid solution by capturing palladium before precipitation of $Pd(OH)_2$ and during its reduction, probably by ammonia formed by decomposition of urea (37). The presence of metallic palladium was indeed confirmed by the X-ray diffractograms of the solid solutions and also by the Pd 3d XPS spectra of the gold-rich samples exhibiting the XPS component at 335 eV, typical of metallic Pd. The ascertained presence of the $Au_{80}Pd_{20}$ phase in all the gold-rich samples may then be responsible for the activity trend shown in Fig. 1. With the increase in the gold percentage, according to Table 2, the formation of the $Au_{80}Pd_{20}$ alloy was favored, until it became the main or only detected phase.

It should be remarked that the data of Table 2 refer to the catalysts in the precursor stage, that is, after calcination. However, these data can still be related to the catalytic behavior because, as indicated in Fig. 6 for selected samples, the subsequent catalyst treatment did not produce a significant change in the alloy structure except for a further reduction of the palladium oxide.

The plateau of Fig. 1 corresponds to a higher activity, per gram of palladium, than the pure monometallic catalyst and is indicative of a positive effect of gold in such palladium catalysts in the HDS reaction of thiophene. Considering the low activity exhibited by the monometallic Au catalyst, the effect of gold would be described as a diluting effect. If the reaction were structure sensitive, the size of the active ensemble would have been rather important and the addition of Au to Pd, by lowering the average sizes of the active Pd ensemble, could have increased the activity (17). Different distribution of the active sites of different intrinsic activity may account for the rather scattered values of the activation energies listed in Table 1.

Differently from the palladium-rich catalysts, the samples with a high gold content did not present evidence of palladium sulfide, as clearly indicated in the X-ray diffractograms of Fig. 5. Moreover, the intensities of the Pd_4S-related peaks decreased noticeably, until complete disappearance for a gold loading above 35 wt%. Figure 6 shows that a direct relation exists between palladium sulfide and free palladium which was present as oxide in the calcined samples. Comparison between the two samples reported in Fig. 6 suggests that for increasing amounts of gold, more palladium is alloyed, with consequently less PdO formation, less free Pd metal, and less or nil Pd_4S.

5. CONCLUSION

A good mixing of the palladium and gold was achieved in the series of Au_xPd_y catalysts supported on ASA by the slow deposition–precipitation method. The X-ray diffraction analysis indicated formation of gold-rich solid solutions of different metal compositions. The preferential nucleation of the gold hydroxides particles on the support was likely to have determined the composition of the bimetallic solution. Palladium, not involved in alloying, was present as PdO crystallites, which were reduced to metallic Pd upon hydrogen treatment. Formation of alloyed particles seemed to be beneficial for the catalytic activity of the HDS reaction of thiophene. The rate constant per gram of palladium increased with gold content up to 50 wt%. The presence of palladium sulfide as Pd_4S was evidenced in the palladium-rich catalysts from the X-ray diffraction analysis of the samples after catalytic tests. In contrast, the gold-rich samples, consisting mainly of the solid solution, did not exhibit such a phase.

In conclusion, the beneficial effect of gold on this series of catalysts appeared to be of a geometrical and structural nature; the geometrical effect would consist of the reduction of the size of the active Pd ensemble by simply diluting the palladium atoms in the Au_xPd_y solid solution. Such an explanation would indicate a structure sensitivity of the HDS reaction. The other effect played by gold would consist of inhibiting the formation of less-active palladium sulfide, Pd_4S, by capturing in its lattice the palladium which, as free metal, would otherwise have a tendency to be sulfided.

ACKNOWLEDGMENT

Support by the European Community, Grant COST, project D 15, is acknowledged.

REFERENCES

1. Kaufmann, T. G., Kaldor, A., Stuntz, G. F., Kerby, M. C., and Ansell, L. L., *Catal. Today* **62**, 77 (2000).

2. Topsoe, H., Clausen, B. S., and Massoth, F. E., *in* "Hydrotreating Catalysis" (J. R. Anderson and M. Boudart, Eds.), p. 3. Springer-Verlag, Berlin, 1996.
3. Furimsky, E., and Massoth, F. E., *Catal. Today* **52**, 381 (1999).
4. Qian, W., Yoda, Y., Hirai, Y., Ishihara, A., and Kabe, T., *Appl. Catal. A* **184**, 81 (1999).
5. Navarro, R., Pawelec, B., Fierro, J. L. G., and Vasudevan, P. T., *Appl. Catal. A* **148**, 23 (1996).
6. Cooper, B. C., and Donnis, B. B. L., *Appl. Catal. A* **137**, 203 (1996).
7. Barbier, J., Lamy-Pitara, E., Marecot, P., Boitiaux, J. P., Cosyns, J., and Verna, F., *Adv. Catal.* **37**, 279 (1990).
8. Vaarkamp, M., Miller, J. T., Modica, F. S., Lane, G. S., and Koningsberger, D. C., *J. Catal.* **138**, 675 (1992).
9. Yoshimura, Y., Yasuda, H., Sato, T., Kijima, N., and Kameoka, T., *Appl. Catal. A* **207**, 303 (2001).
10. Corma, A., Martinez, A., and Martinez-Soria, V., *J. Catal.* **169**, 480 (1997).
11. Caldwell, T. E., Abdelrehim, I. M., and Land, D. P., *Surf. Sci.* **367**, L26 (1996).
12. Haruta, M., and Datè, M., *Appl. Catal. A* **222**, 427 (2001).
13. Bond, G. C., and Thompson, D. T., *Catal. Rev.–Sci. Eng.* **41**, 319 (1999).
14. Haruta, M., *Catal. Today* **36**, 153 (1997).
15. Hayashi, T., Tanaka, K., and Haruta, M., *J. Catal.* **178**, 566 (1998).
16. Johansson, Å., and Stafström, S., *Chem. Phys. Lett.* **322**, 301 (2000).
17. Bond, G. C., and Rawle, A. F., *J. Mol. Catal. A* **109**, 261 (1996).
18. Bonarowska, M., Pielaszek, J., Juszczyk, W., and Karpinski, Z., *J. Catal.* **195**, 304 (2000).
19. Bonarowska, M., Malinowski, A., Juszczyk, W., and Karpinski, Z., *Appl. Catal. B* **30**, 187 (2001).
20. Jan, C.-A., Lin, T.-B., and Chang, J.-R., *Ind. Eng. Chem. Res.* **35**, 3893 (1996).
21. Geus, J. W., *in* "Preparation of Catalysts III" (G. Poncelet, P. Grange, and P. A. Jacobs, Eds.), p. 1. Elsevier, Amsterdam, 1983.
22. JCPDS Powder Diffraction File, Int. Centre for Diffraction Data, Swarthmore.
23. West, A. R., "Solid State Chemistry and its Applications." Wiley, Chichester, UK, 1998.
24. Klug, H. P., and Alexander, L. E., "X-ray Diffraction Procedures for Polycrystalline and Amorphous Materials." Wiley, New York, 1954.
25. Shirley, D. A., *Phys. Rev. B Condens. Matter* **5**, 4709 (1972).
26. Sherwood, P. M. A., *in* "Practical Surface Analysis" (D. Briggs and M. P. Seah, Eds.), p. 181. Wiley, New York, 1990.
27. Venezia, A. M., Raimondi, F., La Parola, V., and Deganello, G., *J. Catal.* **194**, 393 (2000).
28. Pecoraro T. A., and Chianelli, R. R., *J. Catal.* **67**, 430 (1981).
29. Chastain, Ed., "Handbook of X-Ray Photoelectron Spectroscopy" (J. Chastain, R. C. King, Eds.), Perkin–Elmer Corp., Eden Prairie, MN, 1995.
30. La Parola, V., Deganello, G., Scirè, S., and Venezia, A. M., submitted for publication.
31. Dalucu, D., Klemberg-Sapieha, J. E., and Martinu, L., *Surf. Sci.* **472**, 33 (2001).
32. Deki, S., Akamatsu, K., Hataneka, Y., Mizuhata, M., and Kajinami, A., *Nanostruct. Mater.* **11**, 59 (1999).
33. Nascente, P. A. P., de Castro, S. G. C., Landers, R., and Kleiman, G. G., *Phys. Rev. B Condens. Matter* **43**, 4659 (1991).
34. Ponec, V., and Bond, G. C., *Stud. Surf. Sci. Catal.* **95**, 206 (1995).
35. Hensen, E. J. M., Brans, H. J. A., Lardinois, G. M. H. J., de Beer, V. H. J., van Veen, J. A. R., and van Santen, R. A., *J. Catal.* **192**, 98 (2000).
36. Martell, A. E., and Smith, R. M., "Critical Stability Constants," Vol. 4. Plenum, New York, 1976.
37. Lycourghiotis, A., Defossè, C., Delannay, F., and Delmon, B., *J. Chem. Soc. Faraday Trans. 1* **76**, 2052 (1980).